ELSEVIER

Contents lists available at ScienceDirect

#### **Environmental Research**

journal homepage: www.elsevier.com/locate/envres





# Nitrate modulates high CO<sub>2</sub> effects on carbon partitioning in *Gracilariopsis lemaneiformis*: Trade-offs between particulate and dissolved organic carbon sequestration

Jichen Chen <sup>a</sup>, Chi Song <sup>a</sup>, Yicheng Ke <sup>a</sup>, Mengmeng Wang <sup>a</sup>, Jianing Qiu <sup>a</sup>, Liujun Nie <sup>a</sup>, Gang Li <sup>b</sup>, Guang Gao <sup>a,\*</sup>

#### ARTICLE INFO

# Keywords: Carbon sequestration Flue gas Macroalgae Marine CO<sub>2</sub> removal Nitrate availability Recalcitrant dissolved organic carbon Transcriptomic

#### ABSTRACT

Intensive studies have explored the feasibility of using high CO<sub>2</sub> concentrations to culture microalgae for carbon capture. Compared to microalgae, macroalgae are easier to be harvested, thereby reducing culture cost. However, little is known regarding the possibility of using macroalgae to fix and sequester high levels of CO2. In this study, Gracilariopsis lemaneiformis was cultured under low (8  $\mu$ M) and high (200  $\mu$ M) nitrate concentrations to clarify the physiological and molecular responses of carbon fixation and sequestration to a 10 % high CO<sub>2</sub> concentration (HC). HC, inducing low pH, inhibited specific growth rate (SGR) and net particulate organic carbon (POC) production. High nitrate (HN) promoted maximum photochemical efficiency, content of photosynthetic pigments and particulate organic nitrogen (PON), but could not relieve the negative effect of HC and instead led to a further decrease in SGR and net POC production likely by exacerbating cellular C: N imbalances. HC resulted in increased dissolved organic carbon (DOC) and refractory dissolved organic carbon (RDOC) accumulation while HN inhibited the accumulation under HC. Transcriptomic analysis revealed that HC downregulated 56 % of differentially expressed genes (DEGs). Downregulated genes included those involved in the TCA cycle, Calvin cycle, nitrogen assimilation, protein processing and degradation, consistent with HCinhibited growth. Although 41 % of DEGs were upregulated by HN, the combination of HN and HC led to 78 % DEGs being downregulated. The findings in this study indicate that high CO<sub>2</sub> (10 %) reduces net POC production but enhances DOC and RDOC accumulation, with these effects being modulated by nitrate availability. When using macroalgae to capture flue gas-level CO2, attention should be paid to the appropriate concentrations of CO<sub>2</sub> (<10 %) and nitrate (<200 µM). This research provides crucial insights into using CO<sub>2</sub> in flue gas to culture macroalgae for carbon sequestration.

#### 1. Introduction

Continuous increase of atmospheric  $CO_2$  concentration arouses global concerns. Global net anthropogenic greenhouse gas (GHG) emission has been estimated to be  $59 \pm 6.6$  GtCO<sub>2</sub>-eq in 2019, 54 % (21 GtCO<sub>2</sub>-eq) higher than that in 1990, with the largest share and growth occurring in  $CO_2$  from fossil fuels combustion and industrial processes (IPCC, 2023). It is unequivocal that continuously superfluous  $CO_2$  emission has warmed the atmosphere, ocean and land, leading to climate change and extreme weather (Baker et al., 2018; Solomon et al., 2009). Increased  $CO_2$  concentration can trap the outgoing longwave

radiation, leading to lesser heat dissipation (Freese and Cronin, 2021). Climate change has caused substantial damages to terrestrial, cryospheric, freshwater, and marine ecosystems such as mass coral bleaching (Griffith and Gobler, 2020; Mourey et al., 2019; Skirving et al., 2019). Climate change has affected food and water security, human health, livelihoods, and key infrastructure (Al-Jawaldeh et al., 2022; Schnitter and Berry, 2019). Extreme weather, such as heatwaves, heavy precipitation, droughts, and tropical cyclones, can lead to even more severe consequences, including mass mortality events recorded on land and in the ocean (IPCC, 2023). Global temperature will increase by 4 °C in the current high-emissions trajectory (Representative Concentration

E-mail address: guang.gao@xmu.edu.cn (G. Gao).

<sup>&</sup>lt;sup>a</sup> State Key Laboratory of Marine Environmental Science, College of Ocean and Earth Sciences, Xiamen University, Xiamen, 361005, China

b Daya Bay Marine Biology Research Station, South China Sea Institute of Oceanology, Chinese Academy of Sciences, Shenzhen, 518121, China

<sup>\*</sup> Corresponding author.

Pathway 8.5, RCP8.5), resulting in massive and irreversible impacts on terrestrial and ocean ecosystems. Therefore, immediate and substantial reduction of  $CO_2$  emissions is required. Policies and laws addressing climate change mitigation have consistently expanded since the IPCC Fifth Assessment Report. To achieve the temperature goal of the Paris Agreement "the increase in the global average temperature to well below 2 °C above pre-industrial levels and strive to limit it within 1.5 °C", GHG emissions must reach net zero by the middle of the 21st century.

The urge to decrease the atmospheric  $\mathrm{CO}_2$  brings forth various carbon dioxide removal (CDR) approaches such as bioenergy with carbon capture and storage (BECCS), direct air capture (DAC), enhanced weathering (EW), afforestation, and biochar (Mac Dowell et al., 2022). However, using chemical and engineering methods would increase the cost and additional  $\mathrm{CO}_2$  emissions. Considering that the ocean is the biggest active carbon pool in the planet, the conception of ocean-based CDR has been proposed, including coastal restoration, ocean alkalinity enhancement, ocean fertilization, offshore direct air carbon capture and storage, and macroalgae nearshore cultivation (Alevizos and Barillé, 2023; Nawaz et al., 2023).

Macroalgae farming is deemed as an effective marine CDR approach with huge potential, considering its advantages in available area and culture cost (DeAngelo et al., 2022; Watanabe et al., 2024). Macroalgae can grow across all parts of the planet's surface oceans that cover an area of 360 million km<sup>2</sup>, while the available cropland is 46.3 million km<sup>2</sup> (Gao et al., 2025; Schneider et al., 2022). Consensus reviews reported the feasible CDR approach using seaweed farming (Froehlich et al., 2019; Gao et al., 2022; Wang et al., 2023). In China, the seaweed farming removed 605,830 and sequestrated 344,128 tons of carbon from 2015 to 2019, which is deemed an effective CDR approach (Gao et al., 2021). Electricity generation in fossil-fuel power plants accounts for over 40 % of the worldwide CO2 emissions (Cuéllar-Franca and Azapagic, 2015). Therefore, these sources are the main candidates for potential applications in carbon capture and storage (CCS) or carbon capture and utilization (CCU). Intensive studies have been conducted to investigate the possibility of using CO<sub>2</sub> in flue gas to culture microalgae for CCU. The findings demonstrate that high CO<sub>2</sub> concentrations (0.1–30 %) generally promote microalgal growth and carbon capture, whereas concentrations exceeding this range exert inhibitory effects, primarily mediated by acidification stress (Feng et al., 2025). Macroalgae usually live in coastal waters which experience large pH fluctuations. Therefore, they are likely to deal better with extreme pH stress compared to microalgae. Compared to microalgae, macroalgae farming can not only reduce CO<sub>2</sub>-eq GHG emission, but also return a profit of \$50 per tCO<sub>2</sub>-eq, the net profit after all costs (DeAngelo et al., 2022). It is derived from the dry weight of harvested seaweed, which is converted into the amount of CO2 removed from the atmosphere. Few studies have investigated the physiological performance of *Ulva* under high CO<sub>2</sub> levels (Gordillo et al., 2001, 2003). Notably, the high CO<sub>2</sub> concentration (1 %) employed in these studies has not reached flue gas CO<sub>2</sub> levels, and such research has yet to address carbon sequestration or underlying molecular mechanisms. The organic carbon can be converted into CO<sub>2</sub> and returned to the atmosphere due to the labile components. However, partial labile DOC can be transformed to RDOC by microorganisms, which could remain for a long time (Jiao et al., 2024). Macroalgae are a promising CDR solution, but the very conditions of a key application (flue gas CCU) may be detrimental, a paradox the research confronts. The feasibility of culturing macroalgae with high-concentration CO2 (flue gas level) for carbon capture and utilization (CCU) remains poorly understood.

In China, the most commercially important macroalgae *Gracilaria lemaneiformis* possesses the highest capacity in nitrogen removal and carbon sequestration, which contributes to the dual economic and ecological profits (Gao et al., 2021). Furthermore, *G. lemaneiformis* cultivation inhibits harmful blooms, increases dissolved oxygen levels and maintains the phytoplankton community structure (Yang et al., 2015). Despite its economic and ecological significance, critical

knowledge gaps persist regarding its carbon fixation and sequestration capacity when directly cultured with 10 % CO<sub>2</sub> concentration (flue gas). This lack of mechanistic understanding represents a major bottleneck in advancing CCU strategies that integrate macroalgae cultivation with industrial CO2 sources. The applicability of high CO2 seaweed cultivation for achieving dual economic and ecological benefits remains unclear. Seaweed farming offers dual economic and ecological benefits, yet optimal carbon removal pathways remain unclear. Direct culture under flue gas CO2 could significantly reduce costs while enhancing carbon fixation efficiency. Nitrogen availability modulates macroalgal physiological responses to environmental stress, notably by enhancing growth and biomass accumulation during marine heatwave events (Jiang et al., 2024). Moreover, nitrogen is easier to be consumed than phosphorus in algae which is usually a limited factor (Ortega-Blas et al., 2025). The faster nitrogen consumption may be related to the Redfield ratio (N: P = 16: 1). Therefore, we hypothesized that the low pH resulting from a 10 % CO2 concentration would inhibit the growth and carbon fixation of G. lemaneiformis. We further hypothesized that high nitrogen availability would partially mitigate this acid-induced stress by supporting key metabolic and protein processing pathways. To test this hypothesis, G. lemaneiformis was cultured under different CO2 and nitrate concentrations and analyzed via the combination of physiological, biochemical, and transcriptomic methods.

#### 2. Materials and methods

#### 2.1. Seaweed collection and culture conditions

Gracilariopsis lemaneiformis samples were collected from an operational macroalgal cultivation facility. Seawater was maintained at  $17\pm0.5~^{\circ}\text{C}$  for 30 days under controlled laboratory conditions to allow sediments to settle and labile DOC to be consumed. Then the preserved seawater was filtered through a 0.1 µm pore-size ultrafiltration system to completely remove the particulate matter and microorganisms (MUF1580-2T, Midea Group Co., Ltd) (Jiang et al., 2024). Prior to experimentation, G. lemaneiformis was cultured in natural seawater with two antibiotics (penicillin, 400 U·mL $^{-1}$ ; streptomycin, 0.4 mg mL $^{-1}$ ) for two days to reduce bacterial abundance because its proliferation can affect the growth (Gao et al., 2024). A 7-day nitrogen starvation pre-treatment standardized the physiological baselines and enhanced the nitrate responsiveness.

G. lemaneiformis thalli  $(0.5 \text{ g L}^{-1})$  were cultured in 1 L polycarbonate bottles, at the temperature of 17  $^{\circ}\text{C}$  and the light intensity of 100  $\mu$ mol·photons·m<sup>-2</sup> s<sup>-1</sup> with the light: dark cycle of 12 h: 12 h. In this study, both CO2 and nitrate concentrations were manipulated as experimental variables. Considering that coal-fired power plants typically emit CO2 at concentrations of 10-20 % (Feng et al., 2025), we chose a conservative starting level of 10 % CO2 as the high CO2 treatment. Thus, two CO<sub>2</sub> levels were established: 400 ppm (representing atmospheric CO<sub>2</sub> concentration, designated as LC) and 100000 ppm (equal to 10 % CO<sub>2</sub> concentration in flue gas, designated as HC), with the latter supplied from a pure CO2 gas cylinder. The 10 % CO2 treatment is a simplification of flue gas from which other co-contaminants (e.g., NOx, SO<sub>x</sub>) had been removed. Previous research has demonstrated that a nitrate supply of 200  $\mu$ M can improve the growth rate, photosynthesis and antioxidant activity of G. lemaneiformis (Jiang et al., 2024). Thus, two nitrate concentrations were selected: 8 µM (ambient concentration, designated as LN) and 200 µM (high nitrate concentration, designated as HN). The experimental design implemented a  $2 \times 2$  factorial structure with two independent variables: CO<sub>2</sub> (LC/HC) and nitrate (LN/HN). Half of the culture solution was exchanged for fresh filtered seawater with equivalent nutrients every 4 days, which was appropriate in seaweed cultivation system (Jiang et al., 2024). Moreover, nutrients were added to reach the setting levels for each group every two days. CO2 concentrations were maintained by aerating ambient air and 10 % CO<sub>2</sub> that was supplied by a CO<sub>2</sub> enricher (CE100C-2, Ruihua, China) monitoring CO<sub>2</sub>

input in real-time. Before the exchanging of culture media, the fresh sterilized seawater was fully aerated for 4 h to achieve set  $\mathrm{CO}_2$  and pH values, which were verified by a pH meter (Orion STAR A211, Thermo Scientific, the USA).

#### 2.2. Measurement of specific growth rate

Before weighing, the thalli were moved out and blotted gently with tissue paper to remove the surface water until no obvious wetness remained on the tissue (Gao et al., 2016). The fresh weights of *G. lemaneiformis* (days 0, 7, 10, 17, 20, 27, and 30) were measured using an analytical balance (BSA124S, Sartorius, Germany). The weighed thalli were washed with distilled seawater and then returned to the bottle for subsequent cultivation, as drying them would have compromised their viability. The specific growth rate (SGR) was calculated as follows:

SGR 
$$(\% d^{-1}) = \ln(W_2 / W_1) / (t_2 - t_1) \times 100$$
 (1)

Note:  $W_2$  and  $W_1$  represent the fresh weight at times  $t_2$  and  $t_1$  respectively.

#### 2.3. Measurement of chlorophyll fluorescence of photosystem II

Fresh *G. lemaneiformis* (days 0, 10, 20 and 30) with 2 cm long apical tips were prepared for the determination of photosynthetic parameters by multi-color pulse amplitude modulation chlorophyll fluorometer (Multi-Color-PAM, Walz, Germany). Fifteen minutes are sufficient for full dark adaptation which can consume all electrons in plasmoquinone. Two photosynthetic parameters, maximum photochemical efficiency (Fv/Fm) and nonphotochemical quenching (NPQ), were measured after 15 min of dark adaptation, which were consistent with the previous method (Yang et al., 2021).

#### 2.4. Measurement of pigments and phycobiliproteins

On days 0, 10, 20, and 30, approximately 0.05 g (FW) of *G. lemaneiformis* samples were collected and preserved at  $-20\,^{\circ}\mathrm{C}$  untill extraction. The samples were added with 10 mL 95 % ethanol and incubated at 4 °C for 24 h in darkness. The pigment contents were estimated according to the method (Wellburn, 1994). The Chl a and Carotenoid contents (mg·g $^{-1}$  FW) were calculated by the equations as follows:

Chl 
$$a \text{ (mg} \cdot \text{g}^{-1} \text{ FW)} = 13.36 \times A_{665} - 5.19 \times A_{649}$$
 (2)

Carotenoids (mg 
$$\cdot$$
 g<sup>-1</sup> FW) = (1000  $\times$  A<sub>470</sub> + 904.788  $\times$  A<sub>665</sub>   
- 3138.3245  $\times$  A<sub>649</sub>) / 245

Similarly, the phycobiliprotein (PC) and phycoerythrin (PE) contents were measured according to the previous method (Beer and Eshel, 1985). The samples were gground on ice using a glass grinder and extracted with 10 mL of 1  $\times$  PBS buffer (pH = 6.8). Then, the liquid was centrifuged (4 °C, 6000 rpm, 10 min) for the separation of the supernatant. After that, the absorbances of supernatant were measured at 455 nm, 564 nm, 592 nm, 618 nm, and 645 nm. The PC and PE contents were calculated by the following equations:

PC 
$$(mg \cdot g^{-1} FW) = [(A_{618} - A_{645}) - (A_{592} - A_{645}) \times 0.51] / 0.15$$
 (4)

PE 
$$(mg \cdot g^{-1} FW) = [(A_{564} - A_{592}) - (A_{455} - A_{592}) \times 0.2] / 0.12$$
 (5)

#### 2.5. Measurement of POC, PON contents and C: N molar ratio

The *G. lemaneiformis* samples (days 0, 10, 20, and 30) were collected and washed with filtered and sterile seawater. After that, the samples were dried at 60 °C until constant weight. Furthermore, the dried

samples were fumed with concentrated hydrochloric acid to remove the inorganic carbon for 24 h. The processed samples were dried again at 60  $^{\circ}$ C until constant weight. Then, about 0.8 mg samples were pelletized and placed inside tin capsules for further measurement of particulate organic carbon (POC) and particulate organic nitrogen (PON) contents via Elementar Vario EL Cube (Elementar, Germany). The C: N value was the molar ratio of POC: PON. The net POC and PON production was calculated by the following equation:

$$\Delta POC (mg C \cdot g^{-1} FW) = (W_t \times C_t - W_0 \times C_0) / W_0$$
(6)

$$\Delta PON \left( mg \ N \cdot g^{-1} \ FW \right) = \left( W_t \times N_t - W_0 \times N_0 \right) / W_0 \tag{7}$$

Note:  $W_t$  and  $W_0$  represent the FW at days t and 0;  $C_t$ ,  $N_t$ ,  $C_0$ , and  $N_0$  represent POC and PON contents on days t and 0.

#### 2.6. Measurement of DOC and RDOC concentration

Approximately 30 mL of seawater samples were collected for the measurement of dissolved organic carbon (DOC) concentration. The DOC samples were filtered through glass fiber filters (GF/F,  $0.7 \mu m$ ) into Amber Boston Round glass bottles and stored at −20 °C before measurement. The GF/F and bottles were pre-calcined at 450 °C for 4 h. The DOC samples were determined using the Shimadzu total organic carbon analyzer (TOC-LCPH, Shimadzu, Japan) at 680 °C by the combustion catalytic oxidation method. By comparison, the recalcitrant DOC (RDOC) samples were the residual DOC samples which had experienced 60 days of dark incubation at constant 17 °C. Even kept at 4 °C, different concentrations of DOC were easily degraded within 60 days (Liu et al., 2025). During 30 days of cultivation, the physiological state was not consistent in the whole period. Thus, we tried to minimize the gap between different periods. We chose 10 days for the calculation in each period with two-times of medium exchanges. The DOC production rate was calculated using the following equation:

$$DOC\ production\ rate\ \left(\mu M\ g^{-1}d^{-1}\right) = \left(DOC_{t1} - DOC_{t0}\right)/\left(W_{t0}\times 1\right) \eqno(8)$$

Note:  $DOC_{t0}$  and  $W_{t0}$  represent the DOC concentration and fresh weight of days 0, 10, 20 and 30;  $DOC_{t1}$  represents the DOC concentration of days 1, 11, 21, and 31. The DOC production rate shows 24 h of DOC production in different growth stages.

The calculation equation of RDOC transformation rate was put as follows:

RDOC transformation rate (%) = 
$$\left(DOC_{t2} - DOC_{s2}\right) / \left(DOC_{t1} - DOC_{s1}\right) \times 100\%$$
 (9)

Note:  $DOC_{t1}$  and  $DOC_{t2}$  represent the DOC concentration of culture liquid before and after dark treatment respectively;  $DOC_{s1}$  and  $DOC_{s2}$  represent the DOC concentration of seawater before and after dark treatment respectively;

The calculation equations of DOC accumulation ( $\Delta$ DOC) and RDOC accumulation ( $\Delta$ RDOC) were shown as follows:

$$\Delta DOC = \sum_{1}^{t} \Delta DOCt \tag{10}$$

$$\Delta RDOC = \sum_{1}^{t} \left( \Delta DOCt \times \left[ R_{t0} + \left( R_{t10} - R_{t0} \right) \times \left( t - t_{0} \right) / 10 \right] \right) \tag{11}$$

$$\Delta DOCt \left(mgC \cdot g^{-1}FW \cdot d^{-1}\right) = \left[P_{t0} + \left(P_{t10} - P_{0}\right) \times (t - t_{0})/10\right] \big/ B_{0} \times 12 \big/ 1000 \tag{12}$$

Note: t represents the day;  $t_0$  and  $t_{10}$  represent the first and the last days of the section;  $R_{t0}$  and  $R_{t10}$  represent the RDOC transformation rates on the last day during the section where t locates;  $P_{t0}$  and  $P_{t10}$  represent the DOC production rates on the first day and the last day during the section where t locates;  $P_{t0}$  and  $P_{t10}$  represent the biomass on the first day during the

section.

#### 2.7. Measurement of bacterial abundance

Samples (1.6 mL) were collected and mixed with 400  $\mu$ L 2.5 % glutaraldehyde, and then preserved in cryovials at -80 °C. Before measurement, 10  $\mu$ L of water samples were mixed with 990  $\mu$ L sterile water and 5  $\mu$ L of SYBR Green I working solution (50  $\times$  ) for 20 min of staining in the dark. The bacterial abundance (cells·mL $^{-1}$ ) was estimated at an excitation spectrum of 488 nm via the flow cytometer (BD Accuri C6, Accuri Cytometers, the USA) after the dark incubation. To minimize the background noise interference, the threshold was adjusted upward to reduce the number of spurious events until a clear bitmap containing stained bacteria was obtained.

#### 2.8. RNA extraction and library construction

Transcriptomic analysis was conducted at day 30 to assess the response of G. lemaneiformis after undergoing a full cultivation cycle, consistent with standard 30-day harvest intervals in Chinese aquaculture practices. The samples were collected, frozen in liquid nitrogen, and then stored at  $-80\,^{\circ}$ C. RNA was extracted from the algal samples using Trizol Reagent. Then, the quality was determined using the 5300 Bioanalyser (Agilent) and quantified by the ND-2000 (NanoDrop Technologies). The low-quality RNA samples were deleted while the high-quality was kept for the construction of the sequencing library. After that, the RNA was purified and reversely transcribed. The cDNA library was constructed and sequenced by Shanghai Majorbio Bio-pharm Biotechnology Co., Ltd. (Shanghai, China).

#### 2.9. Quality control and de novo assembly

The paired-end reads were trimmed using fastp to implement the quality control (Chen et al., 2018). After that, the Trinity was used for the de novo assembly of clean data (Grabherr et al., 2011). The assembly quality was improved by filtration and assessment by CD-HIT (Fu et al., 2012), TransRate (Smith-Unna et al., 2016) and BUSCO (Benchmarking Universal Single-Copy Orthologs) (Manni et al., 2021). Furthermore, the assembled transcripts were searched against the NCBI protein nonredundant (NR), Clusters of Orthologous Groups of proteins (COG), and Kyoto Encyclopedia of Genes and Genomes (KEGG) (Ogata et al., 1999) databases using Diamond to identify the proteins which that had the highest sequence similarity.

#### 2.10. DEGs analysis and functional enrichment

The differentially expressed genes (DEGs) between two samples/ groups and gene abundance were calculated and quantified by the transcripts per million reads (TPM) method and RSEM (Li and Dewey, 2011). The differential expression analysis was performed with DESeq2 (Love et al., 2014). The DEGs with  $|\log_2 \text{Fold}| \geq 1$  and FDR <0.05 were identified as significantly different expressed genes. Moreover, the KEGG functional-enrichment analysis was performed to analyze metabolic pathways. The sequence data are available in the GEO database with the accession number GSE280440.

#### 2.11. Statistical analysis

All data were shown as the mean value of three independent biological replicates  $\pm$  standard deviation (SD). SPSS software (version 25.0) was used for all data analyses. Repeated measures analysis of variance (RM-ANOVA) and two-way ANOVA (TW-ANOVA) were employed to analyze the effects of culture time, and the effects of  $CO_2$  and nitrate at each time point, respectively, followed by post-hoc analysis (LSD test, p<0.05 as significant difference) or LSD test (p<0.01 as significant difference) if Levene test was not met (Table S1–2). A

confidence interval of 95 % was set for all tests. The figures were constructed using the Origin 8.5, TBtools, and PowerPoint. The quality control and assembly assessment of transcriptomic data were presented in Table S3–4.

#### 3. Result and discussion

### 3.1. Response of growth and photosynthesis to elevated $CO_2$ and nitrate levels

During 30 days of cultivation, the time had a significant interactive effect with CO2 concentration on the SGR according to RM-ANOVA (Table S1). Specific growth rate under the two CO2 conditions both decreased with time, but it had a larger decline under HC (Fig. 1A). According to the TW-ANOVA, the CO2 concentration only had a significant interactive effect with nitrogen concentration on the SGR at the 17th day (Table S2); HN did not affect the SGR under LC but significantly reduced it under HC (one-way ANOVA). In addition, the CO2 concentration exerted a significant effect on the SGR on the 17th, 20th, 27th and 30th days (Table S2). On day 17, HN had no significant effect on the SGR under LC while it showed significant inhibition under HC. HN aggravated the negative effect on the SGR under HC. The SGR under LCLN showed positive values throughout the whole period. Notably, G. lemaneiformis under LCHN presented the only instance of negative growth  $(-0.03 \text{ d}^{-1})$  on day 10. By contrast, G. lemaneiformis under HCLN and HCHN manifested the negative growth on the 10th day, and this negative-growth trend persisted until the 30th day.

It is important to note a key limitation of the transcriptomic analysis presented here: the data were derived from a single sampling point at a late stage of the experiment. As a result, the observed expression profile may reflect a senescent state or cellular stress response under prolonged high-CO2 exposure, rather than capturing dynamic changes across the acclimation process. Therefore, while the data provide valuable insights into the metabolic status under extreme conditions, the results should be interpreted with caution regarding the overarching physiological acclimation of G. lemaneiformis to carbon capture and utilization. The DEGsvaried in three pairs of comparison groups (Fig. 1B). There were 7330 DEGs showing upregulation while 166 showing downregulation under LCHN compared to LCLN. Conversely, HCLN and HCHN had more downregulated than upregulated DEGs compared to LCLN. HCHN had more downregulated and upregulated genes than HCLN. The severe downregulation observed in HCHN vs LCLN indicates the over-pressure under HCHN, reflecting a systemic cellular shutdown. Among the multiple stresses underlying this response, we highlight the C:N imbalance imposed by high nitrogen (HN) as the primary driver: the disproportionately low carbon availability directly limits the synthesis of essential metabolites and structural components, an effect that is exacerbated by high CO<sub>2</sub> stress. Principal component analysis (PCA) was used to depict the response of G. lemaneiformis to different treatments (Fig. S1). Different treatments distributed in different quadrants except for HCLN and HCHN, which had an overlap with each other. Metabolic pathway of TCA cycle is shown in Fig. 1C. There were 58 DEGs related to TCA cycle between the control (LCLN) and treatments (LCHN, HCLN or HCHN) (Fig. 1D). Compared to LCLN, there were 13 upregulated DEGs (with 3.0-6.9 log<sub>2</sub> folds) under LCHN while 31 (3.4-10.3 log<sub>2</sub> folds) and 51 (3.5-12.6 log<sub>2</sub> folds) downregulated DEGs under HCLN and HCHN respectively. All homologous genes of citrate synthase (CS), aconitate hydratase (ACO), isocitrate dehydrogenase (IDH), and succinate-CoA ligase (SUC) catalyzing the synthesis of citrate, isocitrate, 2-oxoglutarate, and succinate, showed significant downregulation under HCHN. Compared to LCLN, HCHN exhibited more severe restrain on the TCA cycle than HCLN.

During 30 days of cultivation, time had a significant interactive effect with  $CO_2$  concentration or nitrogen concentration on Fv/Fm (Table S1). Fv/Fm under all conditions demonstrated a trend of first decrease and then rise while there were larger amplitudes under HC

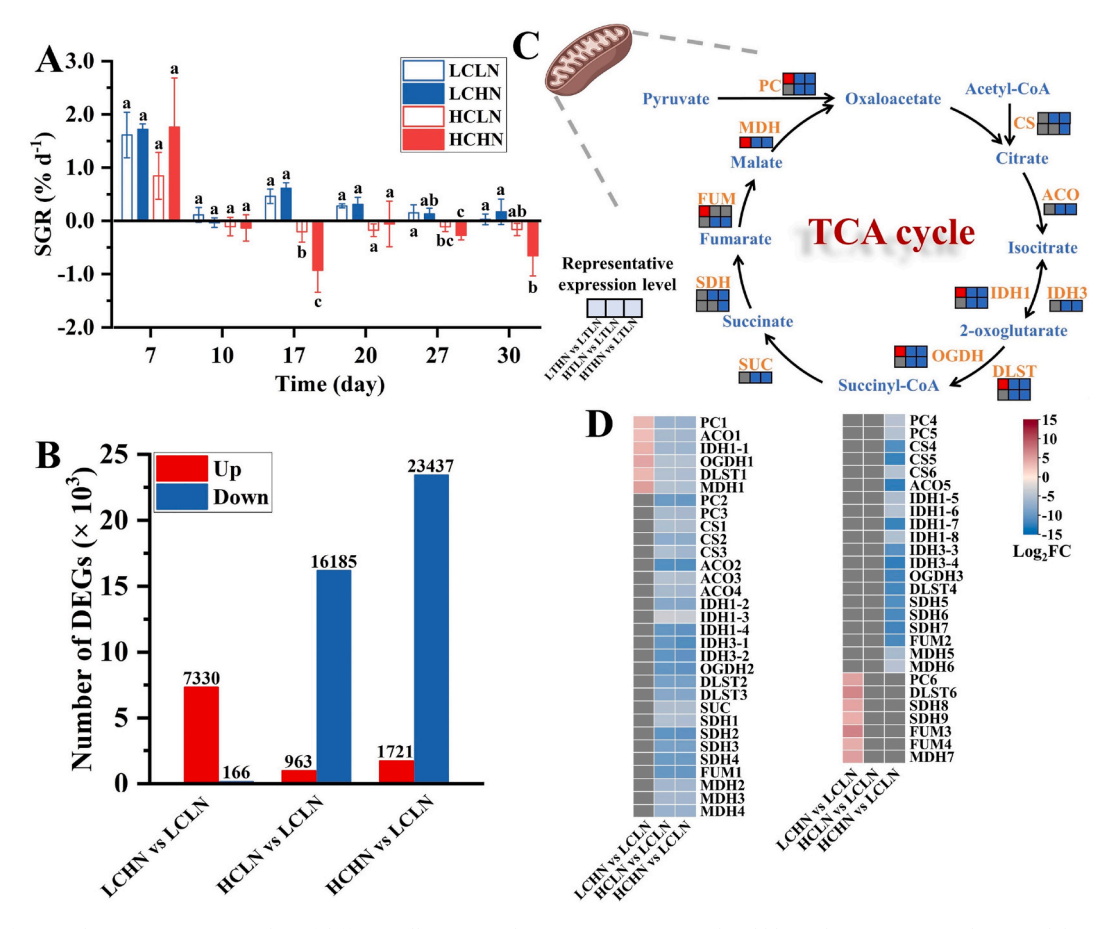


Fig. 1. (A) Specific growth rate (SGR), (B) Number of differentially expressed genes (DEGs); Note: red and blue columns represent the up and down regulation genes. (C) Metabolic pathway of TCA cycle. Note: orange and blue fonts represent gene and intermediate metabolites respectively; Red, blue and gray color blocks represent the representative homology genes with significant upregulation, downregulation and no significant regulation. (D) Heatmap of significant DEGs related to TCA cycle. Abbreviation: ACO, aconitate hydratase; CS, citrate synthase; DLST, dihydrolipoamide succinyltransferase; FUM, fumarate hydratase; IDH, isocitrate dehydrogenase; MDH, malate dehydrogenase; OGDH, 2-oxoglutarate dehydrogenase; PC, pyruvate carboxylase; SDH, succinate dehydrogenase; SUC, succinate-CoA ligase; The numbers after gene name suggests the homologous genes. Note: LC, low  $CO_2$  treatment; HC, high  $CO_2$  treatment; LN, low nitrate level; HN, high nitrate level. The value is the mean  $\pm$  standard deviation (SD), and different letters indicate that there are significant differences among different treatment groups (p < 0.05). Note: red and blue color blocks represent significant up and down regulation; Gray color block represents no significant regulation. (For interpretation of the references to color in this figure legend, the reader is referred to the Web version of this article.)

(Fig. 2A). CO<sub>2</sub> concentration had a significant interactive effect with nitrogen concentration on the Fv/Fm on the 20th day (Table S2); HN did not affect the Fv/Fm under LC but significantly reduced it under HC (one-way ANOVA). By contrast, the CO<sub>2</sub> and nitrogen concentrations had significant effects on the Fv/Fm at 30th day (Table S2); HN significantly enhanced Fv/Fm at both CO<sub>2</sub> conditions. Time had a significant interactive effect with CO<sub>2</sub> and nitrogen concentrations on NPQ (Table S1). NPQ under all conditions decreased with time, with HCHN leading to the largest decline and LCHN having the smallest decline (Fig. 2B). Moreover, CO<sub>2</sub> concentration had significant interactive effects with nitrogen concentration on the NPQ on the 20th and 30th day (Table S2). HN did not affect the NPQ under LC but reduced it under HC on day 20, while HC enhanced the NPQ under LC but reduced it under HC on day 30.

During 30 days of cultivation, time had a significant interactive effect with  $CO_2$  or nitrogen concentration on the Chl a content (Table S1). Chl a content under LCHN showed a rising trend with time while it decreased with time under HC (Fig. 2C). HN enhanced the Chl a content on day 20 and 30 (Table S2). However, HC reduced the Chl a content on the 30th day (Table S2). Time had a significant interactive effect with  $CO_2$  or nitrogen concentration on carotenoid content (Table S1). Carotenoid content under LCHN first decreased, and then had a rising trend while that under HCHN had a decreasing trend with time (Fig. 2D). Nitrogen and  $CO_2$  concentration had significant effects on the

carotenoid contents on the 20th and 30th day, respectively (Table S2). Similar to Chl a content, HN enhanced the carotenoid content on the 20th day, while HC significantly reduced it on the 30th day (Table S2).

During the cultivation period, time had a significant interactive effect with  $\mathrm{CO}_2$  and nitrogen concentrations on the PC content (Table S1). PC content under LC showed a trend of first decrease and then increase while it continuously decreased under HC (Fig. 2E). The  $\mathrm{CO}_2$  concentration had significant effects on the PC content at the 10th and 20th day (Table S2). HC enhanced the PC content on the 10th and 20th day. The time had a significant interactive effect with  $\mathrm{CO}_2$  and nitrogen concentrations on PE content (Table S1). PE content under HC had a larger decrease with time compared with that under LC (Fig. 2F). The  $\mathrm{CO}_2$  concentration had significant interactive effects with nitrogen concentration on the 10th and 30th day (Table S2). HC led to a larger decrease in the PE content under HN compared to LN on day 10; HC did not affect the PE content under LN but dramatically decreased it under HN on day 30. HC also reduced the PE content on day 20.

Metabolic pathway of photosynthesis—antenna proteins is shown in Fig. 2G. There were 44 DEGs related to photosynthesis proteins (Fig. 2H). Compared to LCLN, there were 23 DEGs (3.2–9.1  $\log_2$  folds) under LCHN showing significant upregulation while 28 (4.5–10.1  $\log_2$  folds) and 30 (5.0–10.3  $\log_2$  folds) DEGs showed significant down-regulation under HCLN and HCHN, respectively. There were 15 DEGs of light-harvesting complex related proteins (LHCA, LHCB and LHCsr), 6

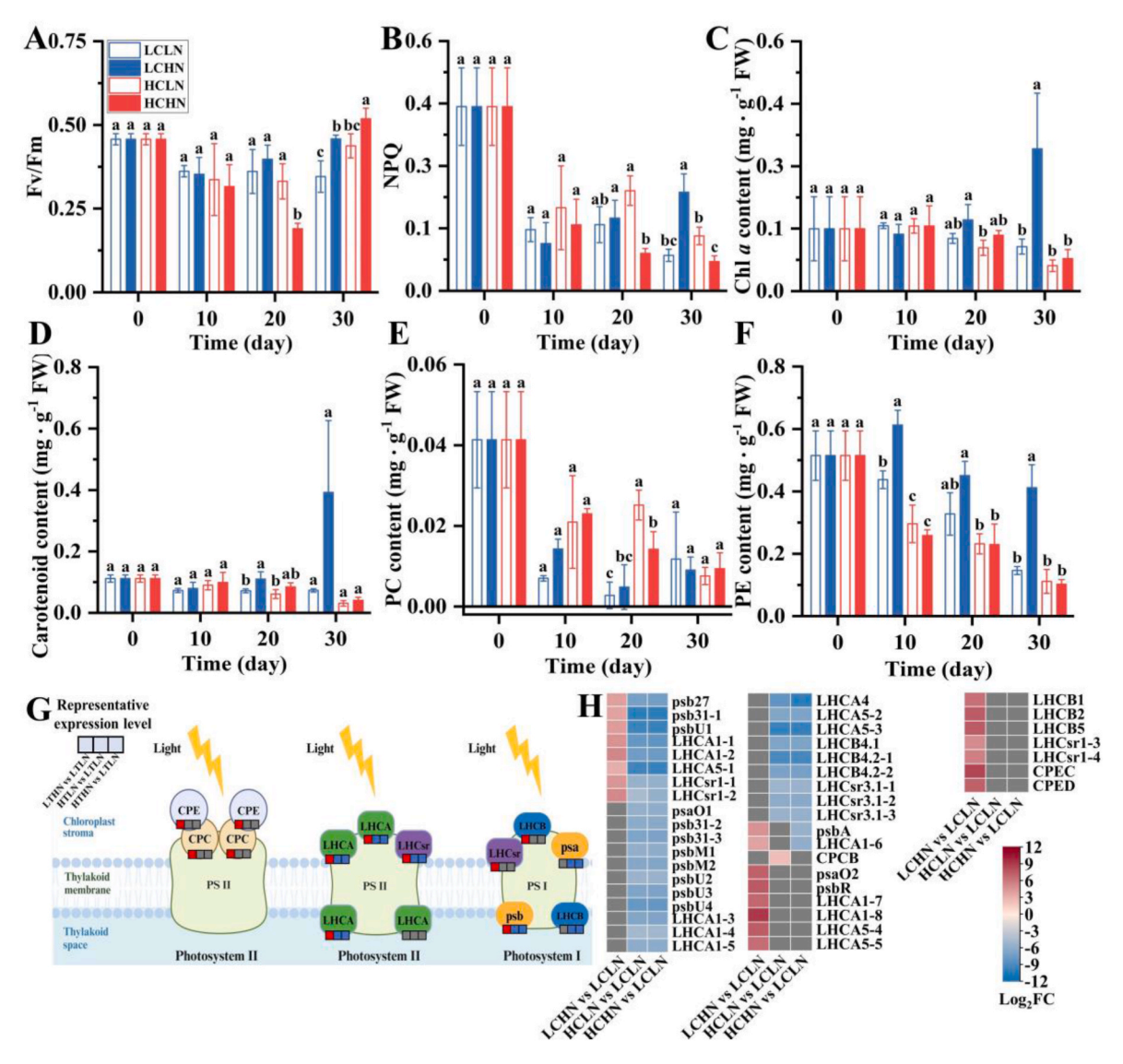


**Fig. 2.** (A) Fv/Fm, (B) NPQ, (C) Chl *a* content, (D) Carotenoid content, (E) PC content, and (F) PE content of *G. lemaneiformis* grown under different CO<sub>2</sub> and nitrate conditions. (G) Metabolic pathway of photosynthesis-antenna proteins. Note as Fig. 1C. (H) Heatmap of significant DEGs related to photosynthesis related protein. Abbreviation: psb, photosystem II repair protein; LHCA, LHCB, light-harvesting complex related protein; LHCsr, light-harvesting complex stress-related protein; CPCB, C-phycocyanin beta chain; CPEC and CPED, phycobilisome linker polypeptide 27.9 kDa, phycoerythrin-associated; The numbers after gene name suggests the homologous genes. Notes as in Fig. 1D.

DEGs of photosystem II repair protein, 2 DEGs of phycoerythrin biosynthesis related proteins (CPEC and CPED) under LCHN showed significant upregulation compared to LCLN. In contrast to LCLN, there was only one DEG related to phycobiliprotein synthesis under HCLN showed upregulation (CPCB,  $\log_2$  folds = 2.3). There were 11 psb and 17 LHC DEGs under HCLN and 12 psb and 18 LHC DEGs under HCHN exhibiting significant downregulation.

The PCA showed that HCLN and HCHN group clusters were very closely, indicateding the overwhelms of HC to HN effects at the transcriptomic level (Fig. S1). Increased CO<sub>2</sub> can commonly stimulate macroalgal growth due to the sufficient carbon supply in ambient environments (Vengatesen et al., 2016). However, the high CO<sub>2</sub> concentration inhibited growth of *G. lemaneiformis*, particularly on day 17 and 27 in the present study. Along with increased CO<sub>2</sub> availability, high CO<sub>2</sub> concentrations can bring about decreased pH. The pH under the high CO<sub>2</sub> condition could be as low as 5.9 while almost 8.1 to 8.2 under LC in the whole period (Fig. S2). Decreased pH can lead to imbalance in acid-base and protons between intracellular and extracellular environments, affecting metabolic activities in cells (Flynn et al., 2012). The

decreased pH would activate the energy consumption to maintain the cellular pH homeostasis via powering ion pumps which inhibited the growth (Taylor et al., 2012). Nearly all DEGs of G. lemaneiformis were downregulated, which suggests the severe inhibition of regular metabolic pathways by HC. Tricarboxylic acid cycle (TCA) and photosynthesis related genes of G. lemaneiformis were significantly inhibited by HC, which is detrimental to growth. On the other hand, the inhibition of growth would reduce the demand of energy which may inhibit the TCA cycle. Environmental stress could block the TCA cycle, followed by decreased energy metabolism and reduced ATP production (Sun et al., 2022). The downregulation of CS may reduce the catalytic efficiency for oxaloacetate and acetyl-CoA which was critical in TCA cycle (Nishii et al., 2023). The overexpression of IDH enhanced the growth, photosynthesis, carbohydrate and lipid content which implied the higher cell viability (Li et al., 2024a). However, the downregulation of IDH can lead to weaker capacity in growth and photosynthesis. Thus, the downregulation of TCA cycle related genes under HC implied the growth restrain. HN aggravated the inhibition under HC on SGR. Low C: N of G. lemaneiformis under HCHN, implied its carbon limitation e.g.

reducing the lipid, carbohydrate and cellular carbon backbone. Thus, the carbon limitation may inhibit the synthesis of essential component of cellular carbon backbone which led to the decrease of SGR. The effects of high  $\mathrm{CO}_2$  levels (higher than 5 %) on macroalgae were understudied. A meta-analysis review shows that high  $\mathrm{CO}_2$  concentrations (0.1–30 %) generally promote microalgal growth (Feng et al., 2025). The physiological traits, e.g., thicker boundary layers and more complex tissues, enable macroalgae to be better adapters compared to microalgae. However, the findings in this study suggest that microalgae can acclimate to high  $\mathrm{CO}_2$  better than macroalgae, likely due to their short generation times. The current study suggests G. lemaneiformis cannot grow well in a  $\mathrm{CO}_2$  condition of 10 %. Therefore, future study should identify the optimal  $\mathrm{CO}_2$  level for the growth of G. lemaneiformis.

Sufficient nitrogen availability can usually promote photosynthetic pigment content in macroalgae since nitrogen is an essential element for nucleic acids, proteins and enzymes (Jiang et al., 2024). HN also significantly promoted the synthesis of Chl a (day 30), carotenoid (day 20 and 30), and PE (day 10 and 30) in G. lemaneiformis in the present study. It may be the reason for the promoted Fv/Fm (day 30) and NPO (day 30). The inconsistent performance of SGR and Fv/Fm on day 30 was mainly due to partial revival of Fv/Fm in apical tip and overall inhibition in growth. The decreased NPO under HC may derived from the injury of photosynthetic system. Higher NPQ under HN represents the capacity of stress-response. Similar to the Fv/Fm, CO2 had no significant interactive effect with nitrogen on the NPQ on day 10 while it showed significant interactive effect on day 20. These results indicate that G. lemaneiformis maintained photosynthetic stability against environmental stress during the first 10 days but exhibited reduced stress resistance thereafter. The Chl a and PE contents under HC had similar variation tendency in the whole period. However, the PE content under LCHN showed the highest content in the whole period while the Chl a content was the highest on day 20 and 30. HN did not promote the Chl a content on day 10 which was inconformity with PE content. Enhanced SGR, Fv/Fm, photosynthetic pigment contents, and upregulated mechanisms for protein processing, carbon fixation etc. indicated the better health of G. lemaneiformis under LCHN. The PE content under LCHN was significantly enhanced on day 30. The CPED (phycoerythrin synthesis related gene) was significantly upregulated under LCHN while no significant regulation under HNHN (Fig. 2H). The different expression level of CPED illustrated the influence of HC under HN. Moreover, the strong inhibition of energy metabolism under HCHN may influence the synthesis of photosynthesis component.

The transcriptome data in the present study show that the photosynthesis and TCA of G. lemaneiformis were significantly promoted by HN. However, HN did not offset the negative effects of HC but intensified the inhibition on SGR (day 17) and the TCA cycle. More downregulated DEGs including antenna protein related genes further confirmed the negative effect of HN combined with HC. HC significantly inhibited the photosynthesis related genes e.g. PS II repair protein genes (psb), which implied the impairement of self-regulating ability in photosynthesis. Previous studies showed that nitrogen enrichment can alleviate environmental stress on macroalgae (Jiang et al., 2024; Krista and Peggy, 2001). The present study indicates that the nitrogen enrichment does not function when environmental stress surpasses a threshold. Instead, it even generates a synergistically negative effect with environmental stressors. Transcriptomic analysis revealed that HN did not mitigate HC-induced adverse effects. The synergistic negative effects of prolonged extreme low pH exposure compromised stress-response capacity, limiting adaptation to concurrent challenges such as C: N imbalance and osmotic stress. On the other hand, the high energy consumption of pH homeostasis, nitrogen assimilation and C: N balance may cause cellular energy deficit especially under the inhibition of energy metabolism (TCA cycle). This phenomenon could be caused by high nitrogen supply which disrupted the balance of cellular C: N molar ratio (Fig. 5B). On day 30, the C: N molar ratio under HCHN was significantly lower than that under LCLN and HCLN. HN further reduced

the C: N molar ratio under HC. Additionally, high  $CO_2$  and high nitrogen concentrations could inhibit the growth of *Chlorella* sp. respectively, which implied the additive effect on growth inhibition of *G. lemaneiformis* (Li et al., 2014).

# 3.2. Increased POC content while decreased net POC production under high ${\rm CO_2}$

Time had no interactive effect with  $\mathrm{CO}_2$  or nitrogen concentration but alone had an extremely significant effect on POC content (Table S1). POC content showed a rising trend with culture time for all conditions (Fig. 3A). Neither  $\mathrm{CO}_2$  nor nitrogen had a significant effect on the POC content (Table S2). Time had no significant interactive effect with  $\mathrm{CO}_2$  or nitrogen concentration on the net POC production (Table S1).  $\mathrm{CO}_2$  concentration had significant effects on the net POC production on the 20th and 30th day (Table S2). LC had higher net POC production than HC during the whole period except for day 10 under HCHN (Fig. 3B); HC significantly reduced the net POC production on the 20th and 30th day, while nitrogen did not have any significant effect during the culture period (Table S2).

Metabolic pathway of Calvin cycle is presented in Fig. 3C. Totally, 89 DEGs related to TCA cycle were detected between the control (LCLN) and treatment (LCHN, HCLN or HCHN) (Fig. 3D). Compared to LCLN, there were 38 upregulated DEGs (2.4-6.8 log<sub>2</sub> folds) under LCHN while 55 (4.7-9.8 log<sub>2</sub> folds) and 77 (1.4-13.0 log<sub>2</sub> folds) downregulated DEGs under HCLN and HCHN respectively. All of the identified homologous genes of fructose-1,6-bisphosphatase (FBP) in HCLN showed significant downregulation compared to those in LCLN. By comparison, all the homologous genes in HCHN of phosphoglycerate kinase (PGK), FBP, transketolase (TKT), ribose-5-phosphate isomerase (RPI), phosphoribulokinase (PRK), showed significant downregulation compared to LCLN. HCHN resulted in more downregulation genes than HCLN in the Calvin cycle. The overexpression of PGK, catalyzing the conversion of 3-Phosphoglycerate (3PGA) to 1,3-Bisphosphoglycerate (1, 3-BPG) in Calvin cycle, enhances the stress resistance capacity in Pyropia haitanensis (Liao et al., 2023). The overexpression of FBP, which mainly catalyze the breakdown of fructose-1,6-bisphosphate (1, 6-FBP) and convert to fructose-6-phosphate (F6P), enhances the fatty acid and biomass accumulation in Nannochloropsis gaditana (Zhang et al., 2024). PRK catalyzes the phosphorylation of ribulose-5-phosphate into RuBP, the substrate of Rubisco, while the loss of PRK function inhibit the photosynthesis (Boisset et al., 2023). The depression of these key enzymes leads to the downregulation of Calvin cycle. These results indicate that carbon fixation was stimulated under LCHN while suppressed under HCLN and HCHN.

Sufficient CO<sub>2</sub> and nitrogen supply usually promotes POC production in marine algae (Heiden et al., 2018; Jiang et al., 2024). The rising trend of POC content with time in all conditions was due to the consistent supply of CO2 and nitrogen. However, HC and HN did not lead to the accumulation of POC in G. lemaneiformis. Conversely, the net POC production of G. lemaneiformis under HC (day 10, 20 and 30) was significantly inhibited, which could be attributed to the adverse effect of low pH. The increased DOC accumulation of G. lemaneiformis under HCLN and decreased net POC production suggested the cell leakage under HCLN. The POC content under HN was obviously lower than that under LN on both CO2 concentration on days 30, though no significant difference. HC obviously inhibited the SGR from day 17-30 (Fig. 1A). The POC content combined with growth difference led to the net POC production difference. High dissolved CO2/carbonic acid concentration, induced by HC input, may enter the cells and change intracellular pH or directly inhibit the cellular processes.

The net POC production kept a rising trend under LC. *G. lemaneiformis* under HCLN had a slight increase from days 10–30. However, the net POC production of *G. lemaneiformis* under HCHN increased from days 10–20 while decreased from days 20–30. It suggested that HN weakened the duration capacity of *G. lemaneiformis* 

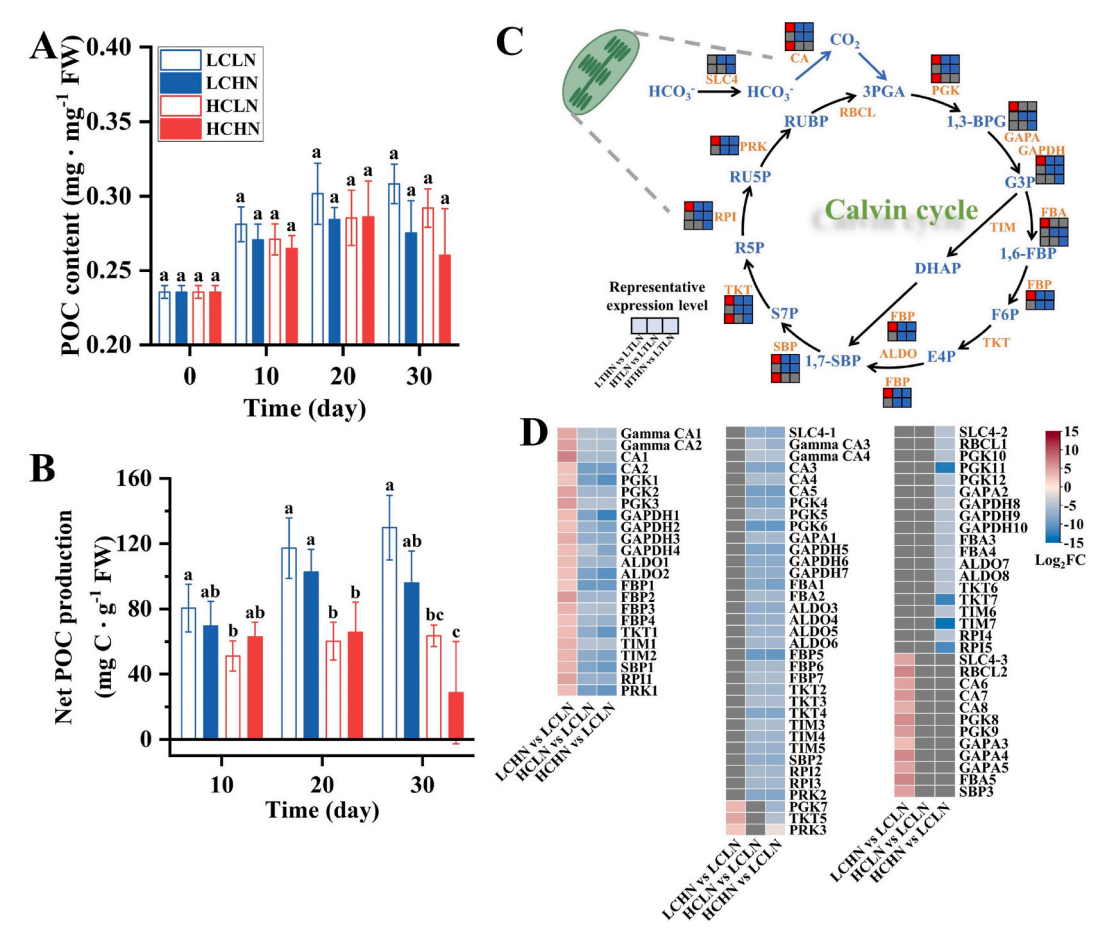


Fig. 3. (A) POC content, (B) net POC production, (C) Metabolic pathway of Calvin cycle. Note as Fig. 1C. (D) Heatmap of significant DEGs related to the Calvin cycle. Abbreviation: CA, carbonic anhydrase; FBA, fructose-bisphosphate aldolase; FBP, fructose-1,6-bisphosphatase; GAPA/GAPDH, glyceraldehyde-3-phosphate dehydrogenase; SLC4, bicarbonate (HCO<sub>3</sub>) transporter; PGK, phosphoglycerate kinase; PRK, phosphoribulokinase; RBCL, ribulose bisphosphate carboxylase; RPI, ribose-5-phosphate isomerase; SBP, sedoheptulose-1,7-bisphosphatase; TKT, transketolase; The numbers after gene name suggests the homologous genes. Notes as in Fig. 1.

under HC, which led to the net POC loss in latter period. The net POC production of coastal plankton communities at low pH (pH = 6.0, equal to the effect of 10 % CO $_2$  treatment) was significantly inhibited, which was similar to our result (Nielsen et al., 2010). Moreover, HN intensified the negative effect of HC on the C: N molar ratio, net POC production and Calvin cycle (day 30). It may be due to the unbalance of cellular C: N molar ratio. *G. lemaneiformis* under HCLN strived to kept carbon assimilation while HN broke the balance and led to its drop down. It concerned about the strong inhibition of growth and carbon fixation. HCLN-induced net POC losses surpassed the RDOC accumulation, while POC remineralization leads to the re-enter of CO $_2$  to atmosphere. This necessitates prioritizing synergistic economic-ecological strategies in seaweed cultivation. The CO $_2$  level of 10 % mightily downregulated the pH level, which strongly influenced the normal activity of *G. lemaneiformis*.

The transcriptomic data revealed that the Calvin cycle of *G. lemaneiformis* under HC was significantly downregulated. It implies that the negative effect of HC on *G. lemaneiformis* crushed the positive effect of CO<sub>2</sub> supply. The RBCL2 (RuBisCO) was significantly upregulated under LCHN while RBCL1 downregulated under HCHN. The different expression pattern of key enzyme RuBisCO demonstrated the low pH effect under HC. The TCA and Calvin cycle related genes were mostly downregulated under HC which demonstrated the inhibition of net POC production under HC. Thus, a proper CO<sub>2</sub> level or regulation of pH could help the net POC production in *G. lemaneiformis*. The cellular PON content of *G. lemaneiformis* was promoted while the C: N molar ratio was reduced by HC on day 30. HC inhibited the net POC production

while promoted the DOC accumulation. The significant enhancement of C: N molar ratio under HCLN indicated the larger loss extent of carbon than nitrogen. The ocean alkalinity enhancement (OAE) can relieve ocean acidification via mitigating the decrease of pH (Burns and Corbett, 2020; James et al., 2023). The high  $\rm CO_2$  level coupled with OAE may help to relieve the pH stress of *G. lemaneiformis* cultivation. There are serval potential approaches related to OAE e.g. injection of alkaline liquid, dispersal of alkaline particles, addition of minerals to coastal environments and the electrochemical removal of acid from seawater (Eisaman et al., 2023). Considering the nearshore cultivation of seaweed, the OAE approach of mineral addition in coastal areas coupled with high  $\rm CO_2$  cultivation may achieve an additive effect in CDR. OAE can alleviate the pH stress of high  $\rm CO_2$  while it does not inhibit the carbon supply.

## 3.3. Response of DOC and RDOC accumulation to different CO<sub>2</sub> and nitrate conditions

Time had a significant interactive effect with nitrogen concentration on the DOC production rate (Table S1). DOC production rate had a sharp decline from day 1–11, and the decline amplitude was larger under LN compared to HN (Fig. 4A).  $\rm CO_2$  and nitrogen concentrations had a significant interactive effect on the first and 31st days (Table S2). HN did not affect the DOC production rate under LC but reduced it under HC on day 1. However, HN enhanced DOC production rate under LC but did not affect it under HC on day 31, indicating that  $\rm CO_2$  and nitrogen had different interactive effects on DOC production in different culture

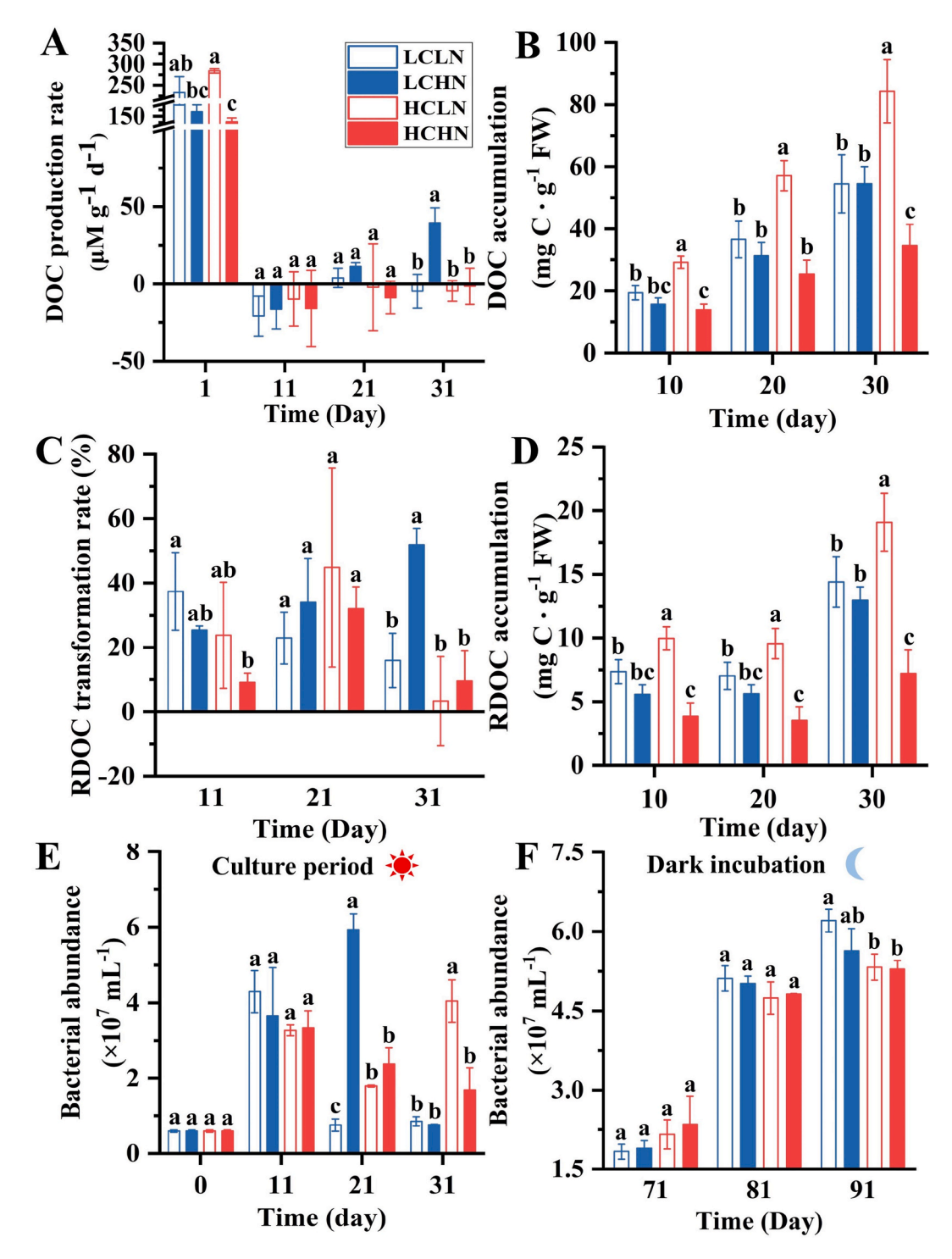


**Fig. 4.** (A) DOC production rate, (B) DOC accumulation, (C) RDOC transformation rate, and (D) RDOC accumulation of *G. lemaneiformis* grown under different CO<sub>2</sub> and nitrate conditions. (E) Bacterial abundance in culture period and (F) Bacterial abundance in dark incubation of *G. lemaneiformis* grown under different CO<sub>2</sub> and nitrate conditions. Notes as in Fig. 1.

periods. Time had a significant interactive effect with  $CO_2$  and nitrogen concentrations on DOC accumulation (Table S1). DOC accumulation at all conditions kept a rising trend with time; HC enhanced DOC accumulation under LN; HN reduced DOC accumulation under HC, and the gap increased with time (Fig. 4B).  $CO_2$  and nitrogen concentrations had significant interactive effects at all time points (Table S2); HC enhanced DOC accumulation under LN at all time points but did not affect it under HN or even reduced it on day 30.

Time had a significant interactive effect with CO2 or nitrogen

concentration on the RDOC transformation rate (Table S1). RDOC transformation rate under LC did not change significantly with time, while it showed a trend of first increasing and then decreasing under HC (Fig. 4C). The highest value of RDOC transformation rate at each treatment varied with time, and it was detected on days 11, 21 and 31 for LCLN, HC, and LCHN respectively. CO<sub>2</sub> and nitrogen concentrations had a significant effect on the RDOC transformation rate on the 31st day (Table S2); HN stimulated RDOC transformation under LC but did not affect it under HC. Time had a significant interactive effect with CO<sub>2</sub> and

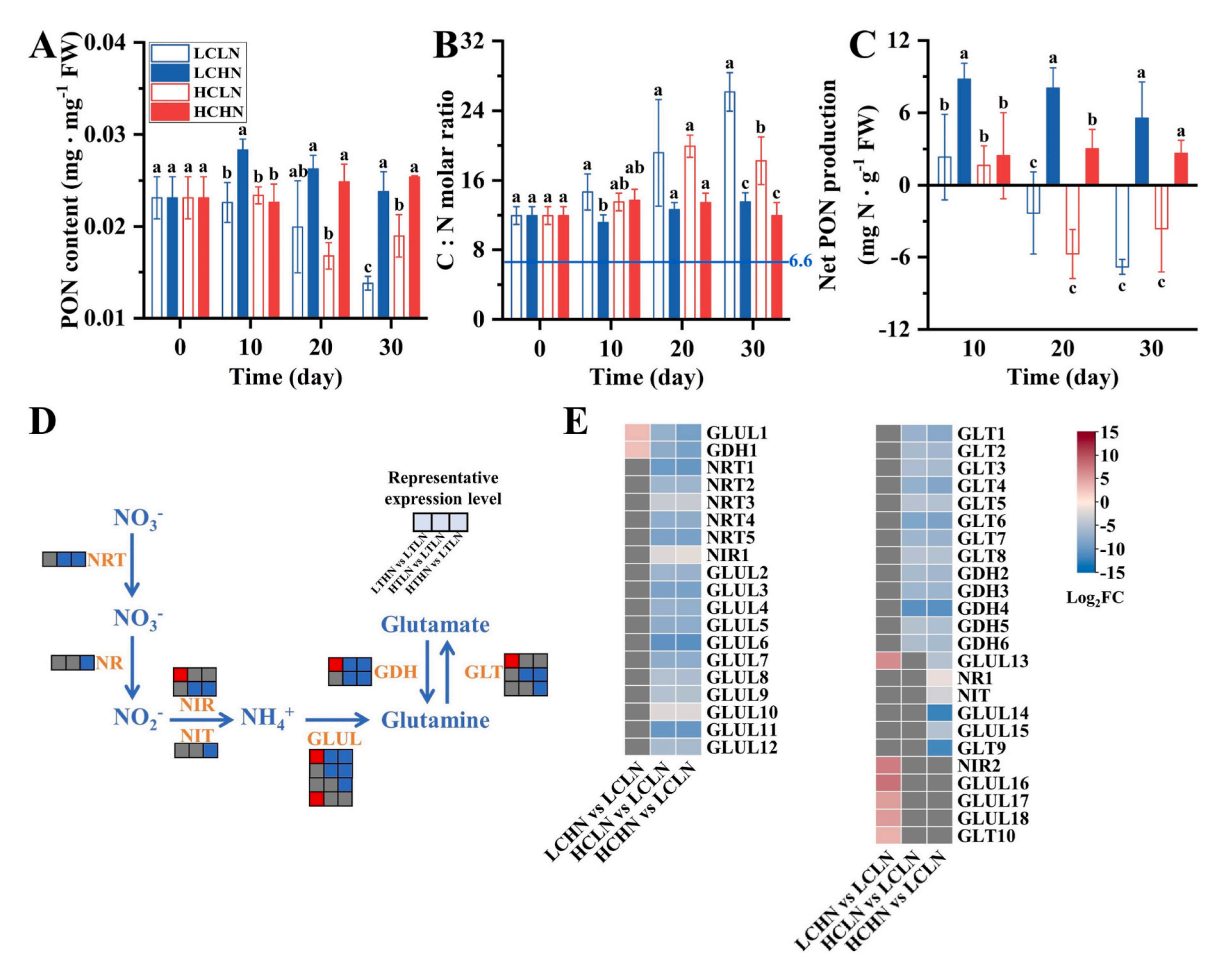


Fig. 5. (A) PON content, (B) C: N molar ratio, (C) net PON production (net gain of nitrogen accumulation), (D) Metabolic pathway of nitrate assimilation. Note as Fig. 1C. (E) Heatmap of significant DEGs related to nitrate assimilation. Abbreviation: GDH, glutamate dehydrogenase; GLT, glutamate synthase; GLUL, glutamine synthetase; NIR, NIT, nitrite reductase; NR, nitrate reductase; NRT, nitrate transporter; The numbers after gene name suggests the homologous genes. Notes as in Fig. 1.

nitrogen concentrations on RDOC accumulation (Table S1). RDOC accumulation kept relatively stable from day 10–20 and had a significant increase by day 30, with the amplitude larger under LN (Fig. 4D).  $\rm CO_2$  and nitrogen concentrations had a significant interactive effect on the RDOC accumulation (Table S2). HC enhanced the RDOC accumulation under LN while reduced it under HN at all time points.

Time had a significant interactive effect with  $CO_2$  and nitrogen concentrations on the bacterial abundance during the culture period (Table S1). The bacterial abundances at all conditions increased from day 0 to day 11 and then demonstrated different patterns, with those under LCLN and HCHN decreasing with time, that under LCHN first increasing and then decreasing, and that under HCLN first decreasing and then increasing (Fig. 4E).  $CO_2$  and nitrogen had significant interactive effects on the bacterial abundance of culture period on the 21st and 31st day (Table S2). HN enhanced the bacterial abundance under LC but did not affect it under HC on the 21st day while HC did not affect the bacterial abundance under LC but reduced it under HC on the 31st day.

Time had an interactive effect with  $\mathrm{CO}_2$  concentration on the bacterial abundance of dark incubation (Table S1). The bacterial abundances of dark period showed an increasing trend, with those under LC having a larger extent (Fig. 4F). Neither  $\mathrm{CO}_2$  nor nitrogen had significant effects on day 11 or 21. On day 31, HC reduced the bacterial abundance (Table S2).

Contrast to the inhibition of net POC production of *G. lemaneiformis* by HC, the DOC production rate (day 31), DOC accumulation and RDOC accumulation were significantly improved during the whole cultivation period. The sharp decline of DOC production in the initial phase could be

attributed to increased bacterial abundance, stimulating the microbial transformation of labile DOC to RDOC. In addition, the low SGR on the 10th day also restrained the DOC production. This suggests that more fixed carbon was transported from intracellular to extracellular in the form of DOC when thalli were cultured in the high CO2 condition. An Arctic mesocosm study showed that increased CO2 concentration could promote the DOC release of phytoplankton (Czerny et al., 2013). However, ocean acidification (850-900 ppm CO2 level) had no effect on the DOC release on seaweed and phytoplankton (Paine et al., 2023; Zark et al., 2015). The concentration of flue gas CO<sub>2</sub> (100000 ppm) is far higher than that of ocean acidification, which caused more intense injury to thalli. Intense injury could stimulate stronger defensive substances or thalli damage which contributed to carbon release. HC did not promote the photosynthesis and carbon fixation but further impaired the growth (Figs. 1A, 2A and 3D). The DOC and RDOC accumulation were mainly due to the injury of frond which led to outflow of cellular organic carbon. Thus, the adverse effect (mainly low pH) of HC promoted the DOC and RDOC accumulation. The DOC could be transferred to RDOC by microbial carbon pump (MCP), catalyzed by microorganisms (Jiao et al., 2024). The transformation of DOC to RDOC via microbial loop enhances the microbial abundance and reinput the nutrients to the ocean. The long time remaining in ocean made RDOC production, via seaweed cultivation, important in capturing CO2. Moreover, the RDOC and refractory POC (RPOC) contribution of seaweed fragments were usually neglected, which occupied a considerable proportion. The liable organic carbon was mineralized and simultaneously produced RDOC (Li et al., 2025). Moreover, the mineralization of seaweed fragments

supports the proliferation of bacteria, virus, and phytoplankton etc. which in turn strengthen the stability of the coastal ecosystem.

Using high CO2 to culture seaweed could not only harvest blue-food but also mitigate climate change. The RDOC transformation rates varied in different treatments and periods. The higher values represent higher refractoriness of initial produced DOC or the higher transformation rate of RDOC via microorganism. However, HN reduced DOC accumulation and RDOC accumulation in G. lemaneiformis under HC in the whole cultivation period. It suggests that HN inhibited the stimulative effect of HC on carbon excretion. HN likely enhanced cell health or membrane integrity sufficiently to mitigate HC-induced carbon secretion. Nitrogen enrichment caused the lower C: N molar ratio which promoted the cellular protein accumulation while inhibited the carbohydrate accumulation in Porphyridium purpureum (Li et al., 2020). Thus, HN could inhibit the carbohydrate accumulation which was main component in DOC (Rehman et al., 2017). Moreover, HN enhanced cellular PON content, leading to decreased C: N molar ratio that is lower than the Redfield ratio (16:1) and that under HCLN. To maintain regular C: N molar ratio, cells need to reduce carbon excretion. This may explain the depression of DOC production under HCHN. A similar phenomenon was also reported for Pyropia haitanensis (Xu et al., 2021). Algae prioritize the self-growth or net POC production when nutrient replete. However, the carbon would be diffused outside the membrane when facing adverse situations.

During the final two-thirds of the culture period, bacterial abundance under HCLN was significantly increased, a trend consistent with the accumulation patterns of DOC and RDOC. The elevated bacterial abundance facilitated the transform of POC to DOC, and ultimately to RDOC. The bacterial abundance in dark incubation on day 91 was significantly inhibited by HC, which implied the lesser DOC to be transformed under HC. It suggested that the DOC was quicker to be transformed under HC. The bacterial abundance in dark incubation under HC was significantly lower than LC, implied the faster degradation or higher proportion of RDOC. RDOC was refractory carboxyl-rich alicyclic molecules (CRAM) which comprised of a complex mixture of carboxylated and fused alicyclic structures with a carboxyl-C: aliphatic-C ratio of 1:2 to 1:7 (Hertkorn et al., 2006). Extracellularly secreted complex polysaccharides, such as fucoidan, were critical component of RDOC (Li et al., 2024b).

#### 3.4. Response of PON and C: N to elevated CO2 and nitrate levels

Time had a significant interactive effect with  $CO_2$  or nitrogen concentration on PON content (Table S1). PON content under LCLN showed a decreasing trend with time, while the trend under HCLN first decreased and then increased; PON content under HN kept a rising trend with time (Fig. 5A).  $CO_2$  concentration had a significant interactive effect with nitrogen concentration on the PON content on the 10th day (Table S2); HN enhanced the PON content under LC but did not affect it under HC. HN decreased the PON content on day 20 but increased it on day 30 (Table S2). Time had a significant interactive effect with  $CO_2$  or nitrogen on C: N molar ratio (Table S1); The C: N ratio under LN showed a rising trend while it maintained relatively stable under HN (Fig. 5B). HN significantly reduced the C: N molar ratio on the 20th and 30th day (Table S2). HC reduced the C: N molar ratio on the 30th day (Table S2).

Time had a significant effect with CO<sub>2</sub> or nitrogen concentration on net PON production (Table S1); Net PON production under LN showed a decreasing trend while it kept relatively stable under HN; Net PON production under HC had a decreasing trend when nitrogen was limited while it kept relatively stable when nitrogen was replete. Nitrogen concentration had a significant effect on the net PON production during the whole period (Table S2); HN significantly enhanced the net PON production under LC during the whole period; HN significantly promoted the net PON production under HC on day 20 and 30 (Fig. 5C). CO<sub>2</sub> concentration had a significant effect on the net PON production on day 20; HN enhanced the PON accumulation while HC inhibited the net PON

production under HN. Metabolic pathway of the nitrate assimilation is depicted in Fig. 5D. In total, the expression of 43 genes in treatment groups was found to have significant differences compared to LCLN (Fig. 5E). Among them, 8 DEGs were upregulated (2.9-7.8 log<sub>2</sub> folds) under LCHN while 32 (2.1–10.6 log<sub>2</sub> folds) and 38 (1.5–12.2 log<sub>2</sub> folds) DEGs were downregulated under HCLN and HCHN respectively. All the homologous genes of nitrate transporter (NRT), nitrate reductase (NR), and glutamate dehydrogenase (GDH) were significantly downregulated in HCHN. The homologous genes of NRT and GDH were significantly downregulated in HCLN. Nitrogen assimilation was slightly stimulated under LCHN but was inhibited under HCLN and HCHN. NRT catalyzes the uptake of extracellular nitrate to intracellular, which influences the nitrogen assimilation rate by controlling the substrate availability. Moreover, NR and NIR (nitrite reductase) catalyze the reduction of nitrate to ammonium which serves as the rate-limiting steps in nitrogen assimilation (Ali, 2020). The downregulation of NRT, NR and NIR indicated the inhibition under HC. However, the inhibition of nitrogen assimilation under HCHN may be due to the inhibition of energy metabolism and SGR. The PON content and net PON production were the reflection of nitrogen assimilation throughout the whole cultivation period. Before day 30, the nitrogen assimilation was activated under LCHN and HCHN which led to the higher PON content. However, nitrogen assimilation was inhibited under HCHN due to excessive cellular nitrogen accumulation, leading to transcriptional downregulation of nitrogen assimilation. HN improved nitrogen assimilation in the early phase, leading to the higher PON contents and lower C: N ratios. However, after reaching the highest value (close to 0.03 mg mg<sup>-1</sup> FW) on day 10, PON content started to decrease, presumably to re-establish a stable C:N balance. This response is supported by transcriptional data that reveal a pronounced down-regulation of nitrogen-assimilation genes at HN on day 30.

#### 3.5. Response of protein processing and degradation

Metabolic pathway of protein processing and degradation pathway is depicted in Fig. 6A. In total, 35 genes of treatment groups were found to have significant differences compared to LCLN (Fig. 6B). Compared to LCLN, there were 33 upregulated DEGs (3.2-9.8 log<sub>2</sub> folds) under LCHN while there were 7 (4.2-12.2  $log_2$  folds) and 9 (5.8-12.4  $log_2$  folds) downregulated DEGs under HCLN and HCHN respectively. The protein processing and degradation were activated by HN, but were inhibited by HC and the combination of HN and HC. HN promoted the nitrate assimilation which enhanced the cellular PON content and net PON production (Fig. 5A and C), which is supported by the activation of protein processing in G. lemaneiformis. The abundant supplies of nitrogen element promoted the protein processing while the oversupply activated the protein degradation mechanism. The protein processing of G. lemaneiformis under HC was significantly inhibited especially the genes of key proteins CRT and UGGT in Endoplasmic Reticulum Quality Control (ERQC). ERQC plays a critical role in correcting misfolded/ unfolded protein caused by stresses (Chen et al., 2022). When ERQC capacity is overwhelmed, ER stress occurs, subsequently activating the UPR (Unfolded Protein Response) and ERAD (ER-Associated Degradation) pathways to eliminate aberrant proteins and restore proteostasis. The upregulation of UPR and ERAD was considered as the capacity in handling stress. The downregulation of critical enzymes CRT and UGGT under HC in ERQC implied its downregulation or impairment which may cause ER stress. However, the ERAD mechanism was not activated or depressed under HC, suggesting the strong impairment of handling misfolded/unfolded proteins. Thus, HC caused strong negative effects on the G. lemaneiformis on protein processing and degradation.

The inhibition of protein processing and the failed degradation mechanism caused by the low pH may lead to the growth inhibition and poor handling of carbon and nitrogen assimilation which influenced the further carbon flow. The strong inhibition of carbon fixation under HCHN likely reduced the availability of carbon skeletons, impairing the

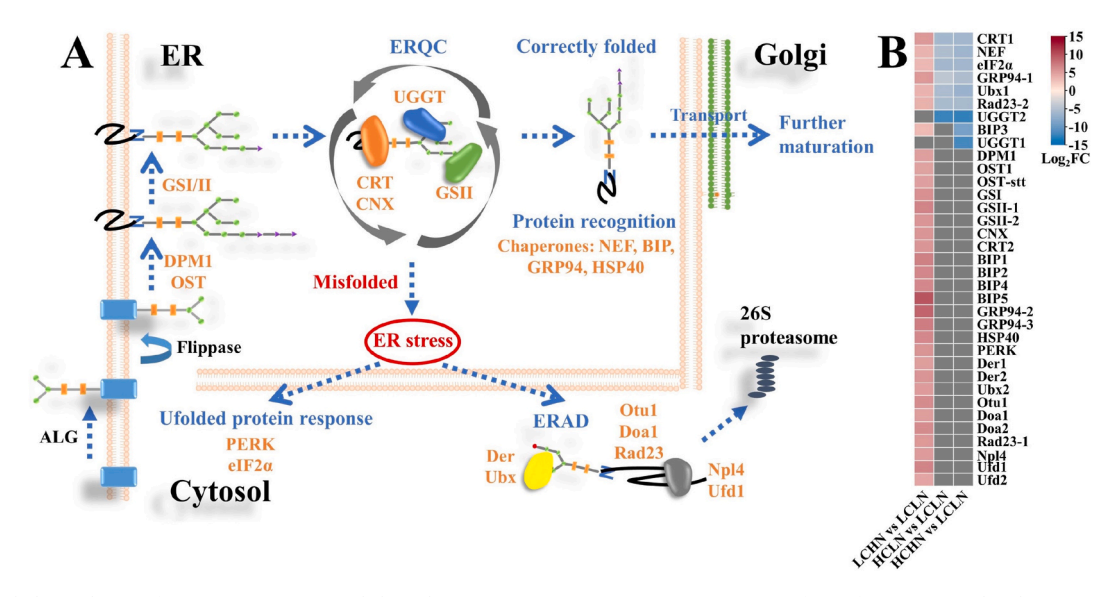


Fig. 6. (A) Metabolic pathway of protein processing and degradation. Notes as in Fig. 1C. (B) Heatmap of significant DEGs related to protein processing and degradation. Abbreviation: BIP/NEF, Heat shock 70 kDa protein; CNX, calnexin; CRT, calreticulin; Der, derlin; Doa1, phospholipase A-2-activating protein; DPM1, dolichol-phosphate mannosyltransferase; eIF2α, translation initiation factor 2 subunit; Npl4, nuclear protein localization protein 4; GRP94, Heat shock 90 kDa protein; GS I/II, Glucosidase I/II; HSP40, Heat shock 40 kDa protein; OST, dolichyl-diphosphooligosaccharide protein glycosyltransferase; Otu1, ubiquitin thioesterase otu1; PERK, eukaryotic translation initiation factor 2-alpha kinase; Rad23, UV excision repair protein Rad23; UGGT, UDP-glucose: glycoprotein glucosyltransferase; Ubx, UBX domain-containing protein; Ufd, ubiquitin fusion degradation protein; The numbers after gene name suggests the homologous genes. Notes as in Fig. 1.

biosynthesis of key enzymes essential for nitrogen assimilation and protein synthesis. Low pH inhibits protein processing and compromises degradation mechanisms, impairing normal protein function. This impairment may lead to growth inhibition, poor carbon and nitrogen assimilation, and ultimately disrupts downstream carbon flux. These molecular responses of *G. lemaneiformis* to HC can explain its physiological performance (e.g., growth, POC and net PON production).

#### 4. Conclusion

In this study, a comprehensive array of physiological, biochemical, and transcriptomic analyses was meticulously carried out to delve into the responses of carbon fixation and sequestration in the economically significant seaweed, G. lemaneiformis, to elevated levels of CO2 and nitrogen. The findings indicate that CO<sub>2</sub> concentrations in flue gas can stimulate the production of DOC and RDOC by G. lemaneiformis, thereby facilitating carbon sequestration at the expense of POC loss. However, this is not a beneficial trade-off between DOC and POC because POC losses exceed DOC accumulation. Furthermore, high CO<sub>2</sub> concentrations are unfavorable for the growth of G. lemaneiformis, which can reduce biomass production when seaweeds are utilized for feed or agar production. This study provides novel insight into the response mechanisms of G. lemaneiformis to the interaction of high CO2 and nitrate concentrations, as well as the utilization of seaweed farming for capturing CO2 from flue gas. Future studies should establish a gradient of CO2 levels to systematically determine the optimal CO2 concentration for the growth of G. lemaneiformis. An optimal CO2 concentration (<10 %) that can strike a balance between carbon sequestration (DOC and RDOC) and biomass production (POC) should be investigated in future studies.

#### CRediT authorship contribution statement

Jichen Chen: Writing – review & editing, Writing – original draft, Supervision, Investigation. Chi Song: Methodology, Investigation, Data curation. Yicheng Ke: Investigation. Mengmeng Wang: Investigation. Jianing Qiu: Investigation. Liujun Nie: Investigation. Gang Li: Writing – review & editing, Visualization, Validation, Supervision. Guang Gao: Writing – review & editing, Visualization, Validation, Supervision,

Project administration, Funding acquisition, Formal analysis, Conceptualization.

#### **Declaration of competing interest**

The authors declare that they have no known competing financial interests or personal relationships that could have appeared to influence the work reported in this paper.

#### Acknowledgements

This work was supported by the National Key Research and Development Program of China (2024YFF0507003), the Open Foundation of Key Laboratory of Marine Environmental Survey Technology and Application, Ministry of Natural Resources (MESTA-2024-A001), the International Cooperation Seed Funding Project for China's Ocean Decade Actions (GHZZ3702840002024020000020), Xiamen University Pingtan Institute (XMUPTI2024001), and the Ocean Negative Carbon Emissions (ONCE) program. The authors also appreciate the support from Google Climate Action Research Awards. Thanks to the PhD Fellowship of the State Key Laboratory of Marine Environmental Science at Xiamen University.

#### Appendix A. Supplementary data

Supplementary data to this article can be found online at https://doi.org/10.1016/j.envres.2025.122897.

#### Data availability

Data will be made available on request.

#### References

Al-Jawaldeh, A., Nabhani, M., Taktouk, M., Nasreddine, L., 2022. Climate change and nutrition: implications for the eastern mediterranean region. Int. J. Environ. Res. Publ. Health 19 (24), 1–27.

Alevizos, E., Barillé, L., 2023. Global ocean spatial suitability for macroalgae offshore cultivation and sinking. Front. Mar. Sci. 10, 1–9.

- Ali, A., 2020. Nitrate assimilation pathway in higher plants: critical role in nitrogen signalling and utilization. Plant Science Today 7 (2), 182–192.
- Baker, H.S., Millar, R.J., Karoly, D.J., Beyerle, U., Guillod, B.P., Mitchell, D., Shiogama, H., Sparrow, S., Woollings, T., Allen, M.R., 2018. Higher CO<sub>2</sub> concentrations increase extreme event risk in a 1.5 °C world. Nat. Clim. Change 8 (7), 604–608.
- Beer, S., Eshel, A., 1985. Determining phycoerythrin and phycocyanin concentrations in aqueous crude extracts of red algae. Mar. Freshw. Res. 36 (6), 785–792.
- Boisset, N.D., Favoino, G., Meloni, M., Jomat, L., Cassier-Chauvat, C., Zaffagnini, M., Lemaire, S.D., Crozet, P., 2023. Phosphoribulokinase abundance is not limiting the Calvin-Benson-Bassham cycle in *Chlamydomonas reinhardtii*. Front. Plant Sci. 14, 1230723.
- Burns, W., Corbett, C.R., 2020. Antacids for the sea? Artificial ocean alkalinization and climate change. One Earth 3 (2), 154–156.
- Chen, J., Du, H., Liu, Z., Li, T., Du, H., Wang, W., Aslam, M., Chen, W., Li, P., Luo, H., Fang, H., Liu, X., 2022. Endoplasmic reticulum-quality control pathway and endoplasmic reticulum-associated degradation mechanism regulate the N-glycoproteins and N-glycan structures in the diatom *Phaeodactylum tricornutum*. Microb. Cell Fact. 21 (1), 1–11.
- Chen, S., Zhou, Y., Chen, Y., Gu, J., 2018. Fastp: an ultra-fast all-in-one FASTQ preprocessor. BIOINFORMATICS. 34 (17), 884–890.
- Cuéllar-Franca, R.M., Azapagic, A., 2015. Carbon capture, storage and utilisation technologies: a critical analysis and comparison of their life cycle environmental impacts. J. CO2 Util. 9, 82–102.
- Czerny, J., Schulz, K.G., Boxhammer, T., Bellerby, R.G.J., Büdenbender, J., Engel, A., Krug, S.A., Ludwig, A., Nachtigall, K., Nondal, G., Niehoff, B., Silyakova, A., Riebesell, U., 2013. Implications of elevated  $\rm CO_2$  on pelagic carbon fluxes in an Arctic mesocosm study an elemental mass balance approach. Biogeosciences 10 (5), 3109–3125.
- DeAngelo, J., Saenz, B.T., Arzeno-Soltero, I.B., Frieder, C.A., Long, M.C., Hamman, J., Davis, K.A., Davis, S.J., 2022. Economic and biophysical limits to seaweed farming for climate change mitigation. Nat. Plants 9 (1), 45–57.
- Eisaman, M.D., Geilert, S., Renforth, P., Bastianini, L., Campbell, J., Dale, A.W., Foteinis, S., Grasse, P., Hawrot, O., Löscher, C.R., Rau, G.H., Renning, J., 2023. Assessing the technical aspects of ocean-alkalinity-enhancement approaches. State of the Planet 2-oae2023. 1-29.
- Feng, Y., Ge, J., Show, P.L., Song, C., Wu, L., Ma, Z., Gao, G., 2025. Using high CO<sub>2</sub> concentrations to culture microalgae for lipid and fatty acid production: synthesis based on a meta-analysis. Aquaculture 594, 1–15.
- Flynn, K.J., Blackford, J.C., Baird, M.E., Raven, J.A., Clark, D.R., Beardall, J., Brownlee, C., Fabian, H., Wheeler, G.L., 2012. Changes in pH at the exterior surface of plankton with ocean acidification. Nat. Clim. Change 2 (7), 510–513.
- of plankton with ocean acidification. Nat. Clim. Change 2 (7), 510–513. Freese, L.M., Cronin, T.W., 2021. Antarctic radiative and temperature responses to a doubling of CO<sub>2</sub>. Geophys. Res. Lett. 48 (17), 1–9.
- Froehlich, H.E., Afflerbach, J.C., Frazier, M., Halpern, B.S., 2019. Blue growth potential to mitigate climate change through seaweed offsetting. Curr. Biol. 29 (18), 3087–3093.e3.
- Fu, L., Niu, B., Zhu, Z., Wu, S., Li, W., 2012. CD-HIT: accelerated for clustering the next-generation sequencing data. Bioinformatics 28 (23), 3150–3152.
- Gao, G., Beardall, J., Jin, P., Gao, L., Xie, S., Gao, K., 2022. A review of existing and potential blue carbon contributions to climate change mitigation in the Anthropocene. J. Appl. Ecol. 59 (7), 1686–1699.
- Gao, G., Gao, L., Jiang, M., Jian, A., He, L., 2021. The potential of seaweed cultivation to achieve carbon neutrality and mitigate deoxygenation and eutrophication. Environ. Res. Lett. 17 (1), 1–14.
- Gao, G., Li, G., Xu, J., Feng, Y., Hall-Spencer, J.M., 2025. Coastal restoration policy needs to consider seaweed diversity. Nature Ecology & Evolution 9, 742–745.
- Gao, G., Zhong, Z., Zhou, X., Xu, J., 2016. Changes in morphological plasticity of *Ulva prolifera* under different environmental conditions: a laboratory experiment. Harmful Algae 59, 51–58.
- Gao, L., Xiong, Y., Fu, F.-X., Hutchins, D.A., Gao, K., Gao, G., 2024. Marine heatwaves alter competition between the cultured macroalga *Gracilariopsis lemaneiformis* and the harmful bloom alga *Skeletonema costatum*. Sci. Total Environ. 947, 1–13.
- the harmful bloom alga *Skeletonema costatum*. Sci. Total Environ. 947, 1–13. Gordillo, F.J.L., Figueroa, F.L.L., Niell, F.X., 2003. Photon- and carbon-use efficiency in *Ulva rigida* at different CO<sub>2</sub> and N levels. Planta 218 (2), 315–322.
- Gordillo, F.J.L., Niell, F.X., Figueroa, F.L., 2001. Non-photosynthetic enhancement of growth by high CO<sub>2</sub> level in the nitrophilic seaweed *Ulva rigida* C. Agardh (Chlorophyta). Planta 213, 64–70.
- Grabherr, M.G., Haas, B.J., Yassour, M., Levin, J.Z., Thompson, D.A., Amit, I., Adiconis, X., Fan, L., Raychowdhury, R., Zeng, Q., Chen, Z., Mauceli, E., Hacohen, N., Gnirke, A., Rhind, N., di Palma, F., Birren, B.W., Nusbaum, C., Lindblad-Toh, K., Friedman, N., Regev, A., 2011. Full-length transcriptome assembly from RNA-Seq data without a reference genome. Nat. Biotechnol. 29 (7), 644–652.
- Griffith, A.W., Gobler, C.J., 2020. Harmful algal blooms: a climate change co-stressor in marine and freshwater ecosystems. Harmful Algae 91, 1–12.
- Heiden, J.P., Thoms, S., Bischof, K., Trimborn, S., Raven, J., 2018. Ocean acidification stimulates particulate organic carbon accumulation in two Antarctic diatom species under moderate and high natural solar radiation. J. Phycol. 54 (4), 505–517.
- Hertkorn, N., Benner, R., Frommberger, M., Schmitt-Kopplin, P., Witt, M., Kaiser, K., Kettrup, A., Hedges, J.I., 2006. Characterization of a major refractory component of marine dissolved organic matter. Geochem. Cosmochim. Acta 70 (12), 2990–3010.
- IPCC, 2023. IPCC, 2023: summary for policymakers. In: Climate Change 2023: Synthesis Report. Contribution Of Working Groups I, II and III to the Sixth Assessment Report of the. Intergovernmental panel on climate change, pp. 1–34.

- James, A., Gately, S.M.K., Jin, Benjamin, Brzezinski, Mark A., Iglesias-Rodriguez, Maria D., 2023. Coccolithophores and diatoms resilient to ocean alkalinity enhancement: a glimpse of hope? Sci. Adv. 9, 1–11.
- Jiang, M., Hall-Spencer, J.M., Gao, L., Ma, Z., Gao, G., 2024. Nitrogen availability regulates the effects of a simulated marine heatwave on carbon sequestration and phycosphere bacteria of a marine crop. Limnol. Oceanogr. 69 (2), 339–354.
- Jiao, N., Luo, T., Chen, Q., Zhao, Z., Xiao, X., Liu, J., Jian, Z., Xie, S., Thomas, H., Herndl, G.J., Benner, R., Gonsior, M., Chen, F., Cai, W.-J., Robinson, C., 2024. The microbial carbon pump and climate change. Nat. Rev. Microbiol. 22, 408–419.
- Krista, K., Peggy, F., 2001. Nitrogen enrichment ameliorates the negative effects of reduced salinity on the green macroalga *Enteromorpha intestinalis*. Mar. Ecol. Prog. Ser. 218, 87–93.
- Li, B., Dewey, C.N., 2011. RSEM: accurate transcript quantification from RNA-Seq data with or without a reference genome. BMC Bioinf. 12 (1), 1–16.
- Li, F., Hu, G., Liu, J., Yuan, C., Zheng, Y., 2014. Lipid production by a CO<sub>2</sub>-tolerant green microalga. Chlorella sp. MRA-1. Journal of Microbiology and Biotechnology 24 (5), 683–689
- Li, H., Zhang, Z., Chen, J., Nair, S., Xiong, T., Zhao, H., He, D., Lee, K., Jiao, N., Zhang, Y., 2025. Fate and carbon sequestration potential of sunken macroalgae in coastal oceans:From long-term microbial degradation perspective. Natl. Sci. Rev. 12 (8), nwa[273.
- Li, J., Wang, W., Li, B., Xue, Y., Wang, X., Liu, S., Hu, S., Tang, J., Yan, B., Li, T., Xue, J., 2024a. NADP(+)-dependent isocitrate dehydrogenase as a novel target for altering carbon flux to lipid accumulation and enhancing antioxidant capacity in *Tetradesmus obliquus*. Bioresour. Technol. 395, 130365.
- Li, S., Ji, L., Chen, C., Zhao, S., Sun, M., Gao, Z., Wu, H., Fan, J., 2020. Efficient accumulation of high-value bioactive substances by carbon to nitrogen ratio regulation in marine microalgae *Porphyridium purpureum*. Bioresour. Technol. 309, 1–9.
- Li, W., Chen, J., Feng, Y., Li, X., Gao, G., 2024b. Production and ecological function of fucoidans from marine algae in a changing ocean. Int. J. Biol. Macromol. 283, 1–14.
- Liao, Y., Ji, D., Xu, Y., Xu, K., Chen, C., Wang, W., Xie, C., 2023. Cloning and functional analysis of a phosphoglycerate kinase (PhPGK) from *Pyropia haitanensis*. J. Appl. Phycol. 35 (4), 1933–1943.
- Liu, T., Li, Y., Shen, Y., 2025. Limited microbial degradation of elevated concentrations of dissolved organic carbon in the deep ocean. Limnol. Oceanogr. 70 (4), 989–1000.
- Love, M.I., Huber, W., Anders, S., 2014. Moderated estimation of fold change and dispersion for RNA-seq data with DESeq2. Genome Biol. 15 (12), 1–21.
- Mac Dowell, N., Reiner, D.M., Haszeldine, R.S., 2022. Comparing approaches for carbon dioxide removal. Joule 6 (10), 2233–2239.
- Manni, M., Berkeley, M.R., Seppey, M., Simão, F.A., Zdobnov, E.M., Kelley, J., 2021.
  BUSCO Update: novel and streamlined workflows along with broader and deeper phylogenetic coverage for scoring of eukaryotic, prokaryotic, and viral genomes.
  Mol. Biol. Evol. 38 (10), 4647–4654.
- Mourey, J., Marcuzzi, M., Ravanel, L., Pallandre, F., 2019. Effects of climate change on high Alpine mountain environments: evolution of mountaineering routes in the Mont Blanc massif (Western Alps) over half a century. Arctic Antarct. Alpine Res. 51 (1), 176–189
- Nawaz, S., Peterson St-Laurent, G., Satterfield, T., 2023. Public evaluations of four approaches to ocean-based carbon dioxide removal. Clim. Policy 23 (3), 379–394.
- Nielsen, L.T., Jakobsen, H.H., Hansen, P.J., 2010. High resilience of two coastal plankton communities to twenty-first century seawater acidification: evidence from microcosm studies. Mar. Biol. Res. 6 (6), 542–555.
- Nishii, M., Ito, S., Osanai, T., 2023. Citrate synthase from Cyanidioschyzon merolae exhibits high oxaloacetate and acetyl-CoA catalytic efficiency. Plant Mol. Biol. 111 (4–5), 429–438.
- Ogata, H., Goto, S., Sato, K., Fujibuchi, W., Bono, H., Kanehisa, M., 1999. KEGG: Kyoto Encyclopedia of genes and genomes. Nucleic Acids Res. 27 (1), 29–34.
- Ortega-Blas, F.M., Ramos-Saravia, J.C., Cossío-Rodríguez, P.L., 2025. Removal of nitrogen and phosphorus from municipal wastewater through cultivation of microalgae Chlorella sp. consortium. Water 17 (8), 1–27.
- Paine, E.R., Britton, D., Schmid, M., Brewer, E.A., Diaz-Pulido, G., Boyd, P.W., Hurd, C. L., 2023. No effect of ocean acidification on growth, photosynthesis, or dissolved organic carbon release by three temperate seaweeds with different dissolved inorganic carbon uptake strategies. ICES (Int. Counc. Explor. Sea) J. Mar. Sci. 80, 272–281
- Rehman, Z.U., Jeong, S., Tabatabai, S.A.A., Emwas, A.H., Leiknes, T., 2017. Advanced characterization of dissolved organic matter released by bloom-forming marine algae. Desalination Water Treat. 69, 1–11.
- Schneider, J.M., Zabel, F., Mauser, W., 2022. Global inventory of suitable, cultivable and available cropland under different scenarios and policies. Sci. Data 9 (1), 1–15.
- Schnitter, R., Berry, P., 2019. The climate change, food security and human health nexus in Canada: a framework to protect population health. Int. J. Environ. Res. Publ. Health 16 (14), 1–16.
- Skirving, W.J., Heron, S.F., Marsh, B.L., Liu, G., De La Cour, J.L., Geiger, E.F., Eakin, C. M., 2019. The relentless march of mass coral bleaching: a global perspective of changing heat stress. Coral Reefs 38 (4), 547–557.
- Smith-Unna, R., Boursnell, C., Patro, R., Hibberd, J.M., Kelly, S., 2016. TransRate: reference-free quality assessment of de novo transcriptome assemblies. Genome Res. 26 (8), 1134–1144.
- Solomon, S., Plattner, G.-K., Knutti, R., Friedlingstein, P., 2009. Irreversible climate change due to carbon dioxide emissions. Proc. Natl. Acad. Sci. 106 (6), 1704–1709.
- Sun, Y., Liu, Q., Shang, S., Chen, J., Lu, P., Zang, Y., Tang, X., 2022. Physiological responses and metabonomics analysis of male and female Sargassum thunbergii macroalgae exposed to ultraviolet-B Stress. Front. Plant Sci. 13, 778602.

- Taylor, A.R., Brownlee, C., Wheeler, G.L., 2012. Proton channels in algae: reasons to be excited. Trends Plant Sci. 17 (11), 675–684.
- Vengatesen, T., Young, C.S., Gobler, C.J., 2016. Ocean acidification accelerates the growth of two bloom-forming macroalgae. PLoS One 11 (5), 1–21.
- Wang, W.-L., Fernández-Méndez, M., Elmer, F., Gao, G., Zhao, Y., Han, Y., Li, J., Chai, F., Dai, M., 2023. Ocean afforestation is a potentially effective way to remove carbon dioxide. Nat. Commun. 14 (1), 1–4.
- Watanabe, K., Tokoro, T., Moki, H., Kuwae, T., 2024. Contribution of marine macrophytes to pCO2 and DOC variations in human-impacted coastal waters. Biogeochemistry 167 (6), 831–848.
- Wellburn, A.R., 1994. The spectral determination of Chlorophylls a and b, as well as total carotenoids, using various solvents with spectrophotometers of different resolution. J. Plant Physiol. 144 (3), 307–313.
- Xu, N., Wang, W., Xu, Y., Ji, D., Chen, C., Xie, C., Xu, K., 2021. Effects of nutrient availability on the release of dissolved and particulate organic carbon by *Pyropia haitanensis* and its implications. Front. Mar. Sci. 8, 1–10.
- Yang, Y., Chai, Z., Wang, Q., Chen, W., He, Z., Jiang, S., 2015. Cultivation of seaweed Gracilaria in Chinese coastal waters and its contribution to environmental improvements. Algal Res. 9, 236–244.
- Yang, Y., Li, W., Li, Y., Xu, N., 2021. Photophysiological responses of the marine macroalga *Gracilariopsis lemaneiformis* to ocean acidification and warming. Mar. Environ. Res. 163, 1–9.
- Zark, M., Riebesell, U., Dittmar, T., 2015. Effects of ocean acidification on marine dissolved organic matter are not detectable over the succession of phytoplankton blooms. Sci. Adv. 1, 1–7.
- Zhang, Z., Li, Y., Wen, S., Yang, S., Zhu, H., Zhou, H., 2024. Metabolomics reveals the impact of overexpression of cytosolic fructose-1,6-bisphosphatase on photosynthesis and growth in *Nannochloropsis gaditana*. Int. J. Mol. Sci. 25 (12), 1–19.